J Appl Electrochem (2013) 43:755–771
DOI 10.1007/s10800-013-0568-8

REVIEW PAPER

Oxygen control technology in applications of liquid lead and lead–bismuth systems for mitigating materials corrosion

Jinsuo Zhang

Received: 14 March 2013 / Accepted: 21 May 2013 / Published online: 8 June 2013

Abstract Oxygen control technology has been successfully applied in liquid lead and lead–bismuth coolant systems for mitigating materials corrosion. In the present study, the development of the oxygen control technology is reviewed. The corrosion mitigation mechanisms, the oxygen control methods, and the oxygen concentration measurements are discussed. The study also analyzes the current technology issues and near future studies needed. For comparisons, the study also reviews other corrosion inhibitors that have also been applied for mitigating corrosion by liquid lead and lead–bismuth.

Keywords Corrosion · Liquid metal · Corrosion inhibitor · Oxygen control

1 Introduction

Liquid lead and lead–bismuth eutectic (LBE, 55 at.% Bi) are good heat transfer mediums and have been applied or considered as the primary coolant candidate in advanced nuclear reactors [1]. Structural materials corrosion by the liquid metal was recognized to be one of the key obstacles [2]. Without protective methods applied, the corrosion rate of a common stainless steel can be in the order of 1 mm year^{-1}, leading to special structural materials being necessary to be developed [3, 4].

The important factors that affect the liquid metal corrosion include the operational, metallurgical, and technological factors [5]. For mitigating the liquid metal corrosion, methods including oxygen control technology, adding metallic corrosion inhibitors, and materials coating have been proposed and studied [6]. Adding a metallic corrosion inhibitor such as Ti and Zr into the liquid metal was reported to be an effective way for mitigating corrosion of carbon steels, but the inhibition performance for corrosion of stainless steels such as HT-9 and T-91 that are cladding material candidates for liquid lead alloy cooled reactors is very low [3]. Material coating leads to a more complex system [7].

The oxygen control technology has been found to be an effective method to mitigate the corrosion of stainless steels by liquid lead and LBE [8]. By carefully controlling the oxygen concentration in the liquid metal, stable oxide films can be formed on the steel surface. The oxide films separate the steel from the corrosive liquid metal, and then the heavy direct dissolution of the steel is inhibited [9, 10]. In last decade, the ongoing activities on corrosion by liquid lead and LBE for the development of advanced nuclear reactor technologies have been focusing on developing methods on how to produce stable oxide protective layers [11]. The oxygen control technology has been well developed and successfully applied to LBE nuclear reactors in Russia [12]. The present article focuses on reviewing the state of the art of the oxygen control technology. The inhibition performance and mechanisms, the oxygen control methods, the target range of the oxygen concentration, and the development of oxygen sensors are reviewed and discussed. The present review also identifies the research gaps and the near future studies needed for practically applying the technology.

2 Oxygen thermodynamics: solubility, activity, diffusion coefficient, partial pressure

The standard Gibbs free energy of formation of an oxide can be expressed by [8]

J. Zhang (✉)
Nuclear Engineering Program, The Ohio State University, 201 W 19th Avenue, Columbus, OH 43210, USA
e-mail: zhang.3558@osu.edu

$$\Delta G_{ox} = A_1 + B_1 T, \quad (1)$$

where A_1 and B_1 are constant and T is temperature in Kelvin. Considering an oxidation reaction of a metal M

$$xM + \frac{y}{2}O_2 \rightleftharpoons M_xO_y. \quad (2)$$

At equilibrium, the standard Gibbs energy of the oxide formation is related to the activities of the reactants and product in Eq. 2 through

$$\Delta G_{ox} = -RT \ln\left(\frac{a_{M_xO_y}}{a_{O_2}^{\frac{y}{2}} a_M^x}\right). \quad (3)$$

For a pure metal and a solid metal-oxide, $a_M = 1$, $a_{M_xO_y} = 1$, and considering $a_{O_2} = p_{O_2}$ in gas with p_{O_2} is the oxygen partial pressure, Eq. 3 can be rewritten by

$$\ln p_{O_2} = \frac{2\Delta G_{ox}}{yRT} = \frac{2B_1}{yR} + \frac{2A_1}{yR}\left(\frac{1}{T}\right) = A_2 + \frac{B_2}{T}, \quad (4)$$

where $A_2 = 2B_1/yR$ and $B_2 = 2A_1/yR$. The measured A_1, B_1 and calculated A_2, B_2 are given in Table 1. Except the data for PbO and Bi_2O_3 using the update measurement [13, 14], the other data are drawn from "the Oxide Handbook [15]."

The dissolution of the oxygen into a liquid metal/alloy can be expressed as the following reaction [16]:

$$\frac{1}{2}O_2(\text{gas}) \rightleftharpoons O[\text{dissolved in liquid}]. \quad (5)$$

The dissolution standard Gibbs energy can be similarly expressed by [16]

$$\Delta G_{sol} = RT \ln\left(\frac{a_O}{P_{O_2}^{1/2}}\right), \quad (6)$$

where ΔG_{sol} is the Gibbs energy of dissolution of gas oxygen into the liquid metal. At the saturation point

$$S_O = \frac{a_O}{\gamma_O} = \frac{1}{\gamma_O}\exp\left(\frac{\Delta G_{ox}}{RT}\right), \quad (7)$$

where S_O is the solubility of oxygen in the liquid metal, a_O and γ_O are the activity and activity coefficient of oxygen in the liquid metal, respectively.

The oxygen solubility in liquid lead and bismuth [17–21] and in LBE [17, 22, 23] has been measured. The solubility can be expressed by

$$\log S_O(\text{wppm}) = A_3 + \frac{B_3}{T}. \quad (8)$$

The constants A_3 and B_3 are given in Table 2. The solubility curves as a function of $1/T$ are given in Fig. 1. The figure indicates that the oxygen solubility in liquid lead, liquid bismuth, and LBE has almost the same magnitude and slope with temperature except the result by IPPE [22] for oxygen in LBE. We cannot make a conclusion that in which liquid the oxygen has high solubility based on the available data. However, we recommend using the most recently data by Ganesan et al. [17] for oxygen in liquid lead and the data by IPPE [22] for oxygen in LBE which has been widely accepted [8].

Table 2 Oxygen solubility (ppm) data

Liquid $\log S_O = A_3 + \frac{B_3}{T}$	A_3	B_3	Temperature (K)	References
Pb	7.42	5,220	783–973	[19]
	6.76	5,600	>1,166	[21]
	7.20	5,100	815–1,090	[17]
Bi	7.84	5,543	<997	[20]
	7.07	4,778	>997	[20]
LBE	5.2	3,400	673–973	[22]
	6.41	4,287	812–1,012	[17]
	7.06	4,774	878–1,073	[23]

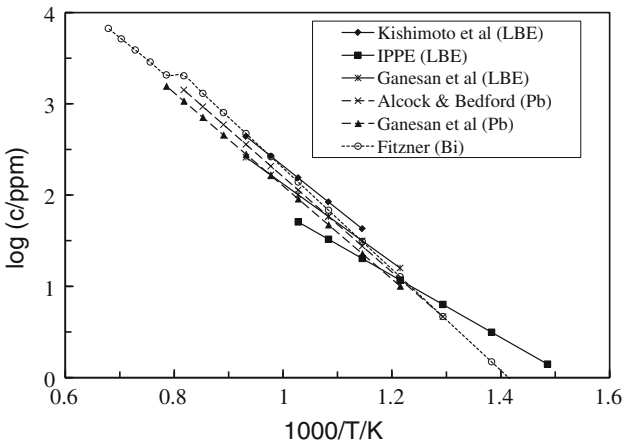

Fig. 1 Curves of oxygen solubility

Table 1 Constants in standard free energy (kJ mol^{-1}) and oxygen partial pressure (atm)

	Bi_2O_3	PbO	NiO	Fe_3O_4	Cr_2O_3	H_2O	Na_2O
A_1	−583.4	−218.98	−237.52	−1,108.3	−1,137.7	−245.57	−420.37
B_1	0.2938	0.09963	0.08804	0.3133	0.2605	0.05445	0.1456
A_2	23.56	23.97	21.18	18.84	20.89	13.10	35.03
B_2	−46,780.5	−52,677.4	−57,137.4	−66,652.6	−91,227.6	−59,073.9	−101,123

The activity coefficient can be calculated by rewriting Eq. 7 when knowing the solubility of oxygen in the liquid metal. The activity coefficients of oxygen in liquid lead, liquid bismuth, and liquid lead–bismuth alloys were also measured (e.g., [24–26]). The available measurements indicated that the activity coefficient depends on not only the operation temperature but also the composition of the liquid metal. For a given temperature, the activity coefficient of oxygen decreases with the content of Pb increasing in the liquid lead–bismuth alloy.

The Gibbs free energies of oxygen dissolution into liquid lead, bismuth, and LBE were also well measured. The most recent data [17, 20] are given in Table 3 and the corresponding curves are given in Fig. 2. The figure indicates that the oxygen dissolves into liquid lead is the easiest process among the three dissolution reactions. Although LBE was composed of 55 at.% Bi, the Gibbs free energy of the oxygen dissolution into LBE is closer to that of liquid lead than to that of liquid bismuth as shown in the figure.

Another important parameter that must be identified is the oxygen diffusion coefficient which determines the movability of oxygen in the liquid metal. The diffusion coefficient has been well measured. Available correlations are given in Table 4 and the corresponding curves are given in Fig. 3. The figure indicates that the data are very scattered. The author recommends the most recent data by Ganesan et al. [17] for oxygen diffusion in liquid lead and LBE, and the data by Fitzner [20] for liquid bismuth which is applicable a pretty large temperature range.

Table 3 Gibbs free energy (J mol^{-1} K^{-1}) of oxygen dissolution

Liquid $\Delta G = \Delta H - T\Delta S$	ΔS (J mol^{-1} K^{-1})	ΔH (J mol^{-1})	References
Pb	−270.4	−1,941,584	[17]
Bi	−154.9	−1,529,048	[20]
LBE	−447.0	−2,038,368	[17]

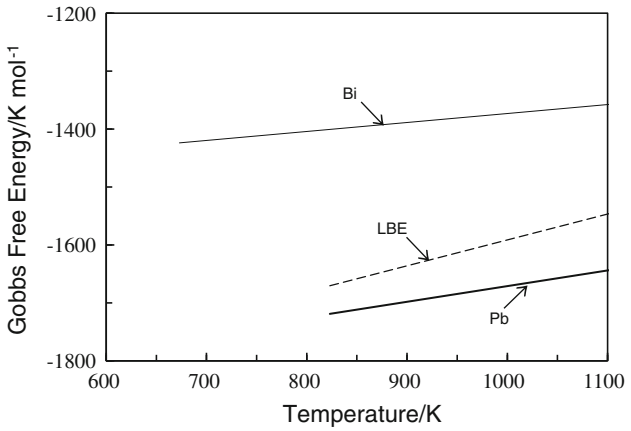

Fig. 2 Curves of the Gibbs free energy of oxygen dissolution

Table 4 Oxygen diffusion coefficient (m s^{-2})

Liquid $D = D_0 \times \exp\left(-\frac{E}{RT}\right)$	D_0 (m s^{-2}×10^7)	E (kJ mol^{-1})	Temperature (K)	References
Pb	1.44	26.04	739–1,080	[21]
	2.79	44.35	818–1,061	[17]
Bi	10.8	49.51	951–1,100	[20]
	0.198	26.71	1,023–1,273	[18]
LBE	1.54 × 10^{-8}	69.11	811–980	[20]

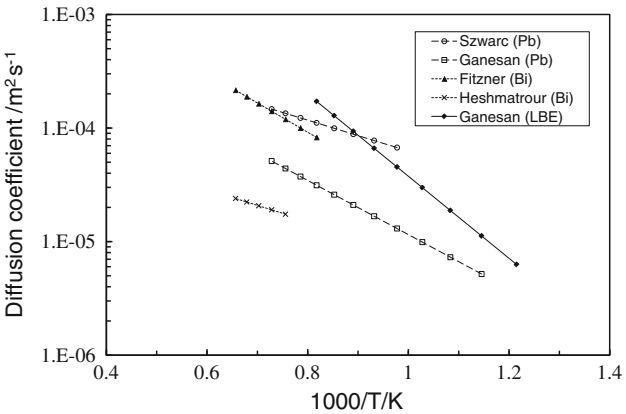

Fig. 3 Curves of oxygen diffusion coefficient

According to Sieverts' law [16], the partial of oxygen pressure for the oxygen dissolution reaction can be expressed by (using $p_{O_2} = 1$ atm as standard condition)

$$P_{O_2}^{1/2}(\text{gas}) = a_O(\text{liquid}) = \gamma_O X_O. \quad (9)$$

With X_O is the concentration of oxygen atom in the liquid with a unity of molar fraction. Therefore, to obtain an expected oxygen concentration, the oxygen partial pressure with a unit of atm needed can be calculated by

$$P_{O_2} = P_{O_2}^s \left(\frac{X_O}{X_O^s}\right)^2. \quad (10)$$

The $P_{O_2}^s$ in Eq. 10 is the oxygen partial pressure needed for the saturation state, and X_O^s is the solubility of oxygen in the liquid metal. For liquid lead, the saturation pressure is the pressure for lead oxide formation which can be calculated by Eq. 4. Using the data given in Table 1

$$\log P_{O_2}^s = 10.41 - \frac{22873}{T}. \quad (11)$$

For LBE, the saturation pressure is the pressure at which the lead oxide starts to precipitate, and can be expressed by

$$\log P^{s}_{O_2} = \frac{2\Delta G_{PbO}}{2.303RT} - \log a_{pb} = 11.17 - \frac{22990}{T}, \quad (12)$$

where a_{pb} is the activity of Pb in LBE, and the expression can be found in Ref. [27].

The relationship between the oxygen pressure and the corresponding oxygen concentration in the liquid metal can be obtained when knowing the saturation oxygen partial pressure. For LBE

$$\log p_{O_2} = 8.77 - \frac{16190}{T} + 2\log c_O \quad (13)$$

with c_O the oxygen concentration in wt%, and liquid lead

$$\log p_{O_2} = 4.01 - \frac{12673}{T} + 2\log c_O. \quad (14)$$

3 Corrosion inhibition mechanisms

The inhibition role of oxygen is to form and maintain a "self-healing" protective oxide films on the structural steel surface which separates the structural materials from the corrosive liquid metal [28]. Unlike other liquid metal coolants such as Na, Li, NaK, and Pb–Li, liquid lead and bismuth are chemically more inert than the major alloying elements (Cr, Fe, Ni) in stainless steels [29], leading it possible to control the oxygen level in a range in which the protective oxide films can be formed on the steel surface without any Pb or Bi oxide precipitation [30].

In a liquid lead or LBE system with oxygen control, two competitive processes occur at the liquid/solid interface, dissolution of steel constituents and oxidation reactions between the steel and the dissolved oxygen [31]. Once an oxide layer forms on the steel surface, the directly dissolution of the steel constituents will be inhibited, and the corrosion–oxidation process in liquid lead and LBE can be simply illustrated in Fig. 4. The steel constituents diffuse through the oxide layer to the oxide/liquid interface where new oxide layer may be formed through reactions with oxygen supplied from the liquid metal. Simultaneously, the metal atoms can also dissolve into the liquid and are transported to other locations by the liquid metal flow [32].

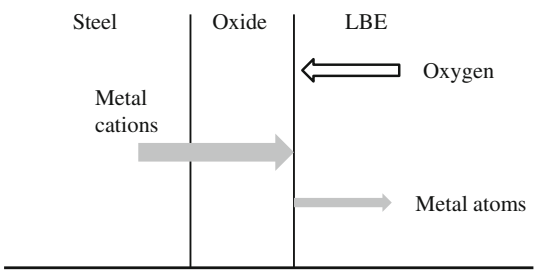

Fig. 4 Transport of oxygen and metal elements through oxide liquid metal [8]

Available experimental results have shown that liquid lead and LBE does have effects on the formation of the oxide layer [33, 34]. The oxide layer structure depends on the oxygen level, the steel composition, the operation temperature, and the hydraulic factors [35]. Generally, there are two possible structures for martensitic steels according to the available experimental results [3, 11]:

(1) For temperatures below 550 °C, the oxide layer structure is composed of an external magnetite layer, Fe_3O_4, and a compact internal Fe–Cr spinel oxide layer. While in other cases, the external magnetite layer was not observed. Penetrations of lead are sometimes observed in the outer layer. The duplex-layer oxide film can protect steels from dissolution.
(2) For temperatures above 550 °C, an internal oxidation zone with oxide precipitates along grain boundaries is observed below the Fe–Cr spinel layer.

Austenitic steels have more Cr and Ni than martensitic steels. The oxide layer formed on austenitic steels has following possible structures [3, 35]:

(1) For temperature below 500 °C, the oxide layer is very thin and is composed of the single-layer Fe–Cr spinel, which can prevent direct dissolution.
(2) For temperature around 550 °C, the oxide layer can have either a duplex- or a single-layer structure, depending on the surface and operation conditions. The duplex-layer can prevent steel component dissolution, while heavy dissolution was observed when the single-layer forms.
(3) For temperatures above 550 °C, heavy dissolution occurs.

Considering the scale removal due to the dissociation of the protective layer into the liquid metal, the possible oxide structures of stainless steels (martensitic or austenitic steels) in liquid lead alloys with oxygen control are shown in Fig. 5 [35].

Initially, a very thin oxide layer forms on the steel surface quickly if the steel is exposed to oxidizing environments without protection. After the thickness reaches 2–3 nm [36], the oxidation reaction slows down and the metal or the oxidant diffusion through the layer formed at the beginning controls the oxidation process. In an oxygen controlled liquid lead or LBE system, the steel can be removed by the liquid with a certain rate. If the removal rate is greater than the diffusion rate of the solid metal through the layer, no new oxide can be formed at the outer surface (liquid/oxide interface), but it is still possible for oxide layer to be formed at the oxide/steel interface because of the inward diffusion of oxygen [37, 38]. For Fe–Cr–base steels, the Fe–Cr spinel formed at the beginning can retain Cr and Ni at their original locations because

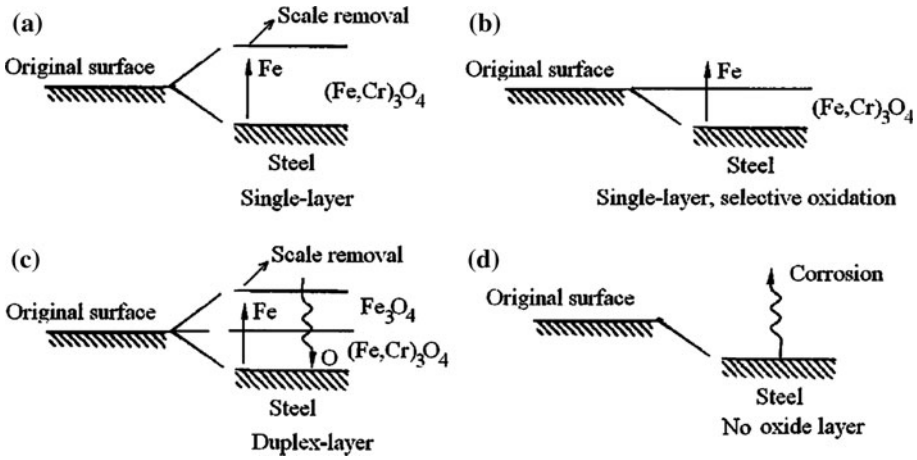

Fig. 5 Possible oxide layer structure of stainless steels in liquid lead alloys with oxygen control [35]

Cr and Ni have smaller diffusion coefficients in Fe–Cr spinel than Fe [36]. Fe diffuses outward and is taken away at the liquid/oxide interface by the flowing liquid (Fig. 5b).

When the rate of Fe reaching the liquid/oxide interface through diffusion is larger than the rate of Fe removed by the flowing liquid, the excess Fe will be oxidized and new oxide layer will be formed at the liquid/oxide interface. Thus, an oxide layer with a duplex-layer structure forms on the steel surface (Fig. 5c). According to the experimental results from gaseous and aqueous solution environments [39, 40], it appears that the inner-/outer-oxide layer interface almost coincides with the original steel surface. The mechanism of a duplex-layer structure oxide film formation is very complicated and is not well understood even in gaseous environments [36]. In a very simple manner, it can be depicted as [41]: Fe diffuses outward through each of the oxide layers and produces a pure iron oxide layer at the liquid/oxide interface. The limited Cr-diffusion leads to Cr-enrichment in the spinel layer near the oxide/alloy interface. Simultaneously, oxygen goes inward through the outer oxide layer and leads to an inner spinel oxide layer formation. Since the oxygen self-diffusion coefficient in the oxide layer is very small, there should be fast paths for oxygen to arrive at the inner layer at sufficiently high rates to account for the observed inner oxide growth [39].

Based on the oxidation mechanisms in gaseous environments and available oxidation data in liquid lead and LBE, the development of the oxide layer with operation time in liquid lead or LBE can be described as shown in Fig. 6 [42, Yeliseyeva (2005) Private discussion]. When a fresh steel is put into a liquid lead or LBE, the Fe-flow toward the liquid appears. As a result, the Fe–O oxide grows over the original surface and opposite flow of cation vacancies is initiated. Structural defects (grain boundaries, sub-boundaries, dislocations, twins, etc.) are the main diffusion sinks for vacancies. Thus, the network of micro-channels is formed gradually in the steel near the surface which can serve as the fast path for oxygen to enter into the oxide layer. Oxygen diffuses along the micro-channels and reacts with active alloying elements such as Cr, which leads to the inner oxidation formation. Thus with time evolution, the duplex oxide layer is formed on the steel surface.

If the oxygen concentration in the liquid metal is too low to form the protective oxide layer, heavy dissolution or corrosion occurs (Fig. 5d) since most of the steel components have high solubility in the liquid metal. Such corrosion can also occur at high temperatures if the oxide layer cannot prevent steel components from dissolution. It is important to notice that the oxide layer structure strongly

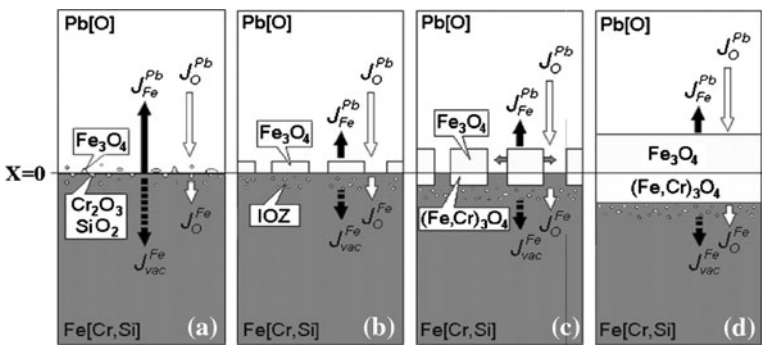

Fig. 6 The duplex oxide origin and evolution on the steel surface during contact with liquid lead/LBE with oxygen control ($X = 0$: initial surface "solid metal/liquid") [42]

depends on the steel composition, such as contents of Cr and Si [43].

4 Inhibition performance

A corrosion model [35, 44] shows that the corrosion rates by liquid lead and LBE are proportional to $c_O^{-4/3}$(c_O is the oxygen concentration in the liquid), which indicates that corrosion rate decreases with increasing the oxygen concentration. The corrosion rate in an LBE loop was calculated for different oxygen concentrations [45]. At a low oxygen concentration (e.g., $c_O = 0$ for calculation), the corrosion rate at the highest temperature (550 °C) of a non-isothermal LBE loop can reach as high as several millimeters per year. Active oxygen control can significantly reduce the corrosion rate [8]. If the oxygen level is maintained at a level of 0.01 ppm, the maximum corrosion rate is about 0.015 mm year^{-1}, which is more than 100 times less than that of a low oxygen concentration case. When the oxygen level is increased to 0.1 ppm, the corrosion rate can be further reduced to a value of 0.0007 mm year^{-1} [45].

Recent studies have focused on characterizing the properties of the oxide layer formed in LBE environments and finding techniques to enhance the protective efficiency. The protective oxide layers of both austenitic steels [41, 46–51] (e.g., ss316, D-9) and martensitic steels [41, 50, 52–54] (e.g., HT-9 and T-91) in liquid lead and LBE have been studied. Critical review of the available experimental data has been done [11], and the corrosion rates and the asymptotic layer thicknesses for different steels were calculated based on the experimental measurements and a theoretical model [3]. The results are given in Table 5 [3]. The table indicates that even for the same operation condition different steels have different corrosion rates, indicating that the inhibition efficiency depends on not only the oxygen concentration but also the steel compositions. From a materials perspective, the higher the concentrations of alloying elements that can form stable, adherent, and dense oxides are, the lower the oxidation/corrosion rate will be. Consequently, for ferritic/martensitic steels, higher concentrations of Cr, Si, or Al result in lower oxidation rates and thinner protective oxide layers [55]. Therefore, alloying steel with Si and Al at the surface area is expected to reduce the corrosion and oxidation rate in an LBE system with oxygen control.

The Russian steel EP823 [56] has the best compatibility with LBE among steels tested at the same condition as shown in Table 5. The corrosion rate is 0.0049 mm year^{-1} and the asymptotic oxide film thickness is 35.8 μm at a temperature of 467 °C for an oxygen concentration of ~0.01 ppm. The HT-9 steel, which has been considered to be a candidate for cladding materials for advanced nuclear reactor of Japan and US LBE-cooled reactors, also has good compatibility. The corrosion rate is 0.011 mm year^{-1} at 460 °C and 0.033 mm year^{-1} at 550 °C. As shown in the table, the asymptotic thickness of the protective coating for HT-9 at this test condition is 52.9 and 73.2 μm at 470 and 550 °C, respectively. The thickness of the oxide film is a concern because a thick oxide layer has a tendency to spall.

An ideal protective layer should be pore-, crack-, and stress-free at high operation temperatures [57]. For practical liquid lead and LBE systems, it is nearly impossible to attain such an ideal protective layer throughout the primary

Table 5 Corrosion and oxidation rate of steels in flowing LBE estimated based on available experimental data by a corrosion model

Steel	T (K)	∇T (K)	V (m s^{-1})	Oxygen (ppm)	$k_p \times 10^{17}$ m^2 s^{-1}	R_C		δ_s (μm)
						×10^{12} m s^{-1}	mm year^{-1}	
T91	743	210	1.9	0.01–0.02	5.043	1.052	0.033	23.9
Optifer	743	210	1.9	0.01–0.02	10.51	1.781	0.056	29.5
EP823	743	210	1.9	0.01–0.02	1.124	0.1572	0.0049	35.8
BA27	743	210	1.9	0.01–0.02	3.72	0.75	0.0236	24.8
BA28	743	210	1.9	0.01–0.02	3.048	0.1639	0.0052	93.0
EM10	743	210	1.9	0.01–0.02	6.143	0.2942	0.0093	104.4
316	823	–	0.5	0.01	10.36	1.523	0.048	34.0
1.4790	823	–	0.5	0.01	15.62	1.374	0.043	56.9
HT9	733	300	1.9	0.02–0.03	3.754	0.3546	0.011	52.9
HT9	823	300	1.9	0.02–0.03	14.8	1.01	0.031	73.2
D9	823	300	1.9	0.02–0.03	6.87	0.704	0.022	49.0

T, temperature; ∇T, temperature difference in the test loop; V, flow velocity; k_p, parabolic oxidation constant; R_C, corrosion rate; δ_s, asymptotic layer thickness

Table 6 Corrosion descriptions and issues and solutions

Corrosion	Status	Issues and solutions
Uniform corrosion	Has been studied a lot experimentally and theoretically.	The oxygen concentration has to be carefully controlled to keep the protective film stable and to avoid heavy oxidation and lead oxide precipitation
Pitting corrosion	Experimental data have been reported on such corrosion, but no analysis has been done	Spallation of oxide film can lead to pitting corrosion, while pitting corrosion can result in more cracks. Keeping the oxide film stable is a good method to avoid pitting corrosion
Stress cracking corrosion	No studies available for an LBE system, but there are lots of studies for other corrosive liquids such as aqueous solutions with carbon dioxide	Studies should be carried out on corrosion at the section where there is stress accumulation such as at bends and wield junctions
Chemical corrosion	Has been studied a lot, especially oxidation corrosion	Control the coolant chemistry by developing and installing a purification system. More studies are needed to identify the impurity interactions and transport in a non-isothermal LBE loop
Dissimilar mass transfer	No study has been reported	Can be avoided by fabricating the loop with one material
Thermal gradient mass transfer	A theoretical model has been developed. The mass transfer properties are well known	Cannot be avoided in a nuclear coolant loop because the loop is non-isothermal. Control by oxygen control
Corrosion product precipitation	Has been reported theoretically and experimentally. But there is no information about its effects on the oxide film stability and the precipitation properties	More studies are needed
Corrosion fouling	No studies reported	The effects of corrosion fouling at the heat exchanger in a LBE system have to be understood for the design of the energy conversion system

coolant loop of an LBE-cooled nuclear reactor. However, based on available experimental data it is possible to achieve acceptable performance by controlling oxygen level in the liquid metal, by selection of the steel composition and surface conditions, and by attention to the system configuration and operating conditions [56].

Although the oxygen control technology for mitigating corrosion in liquid lead and LBE coolant systems has been well developed and experimental data have shown that it has high corrosion inhibition performance, there are still corrosion issues related to the oxygen control technology. These issues, the current status of the issues and the potential solutions are summarized in Table 6. Based on the table, the following four aspects related to corrosion need more studies: (a) oxide film stability, (b) coolant chemistry control, (c) stress corrosion cracking, and (d) corrosion precipitation and fouling.

5 Operation oxygen range

Commonly, the upper limit of oxygen in LBE is set to be the oxygen solubility given by Eq. 8, and the lower limit is determined by the formation of Fe_3O_4 [8]. In LBE with oxygen dissolved, the formation reaction of magnetite is

$$3Fe + 4O \rightarrow Fe_3O_4 \tag{15}$$

and the oxygen potential needed at equilibrium is

$$\log p_{O_2} = \frac{\Delta G_{Fe_3O_4}}{4.606RT} = 8.18 - \frac{28941}{T}. \tag{16}$$

Then according to Eq. 13, the lower limit of oxygen concentration (wt%) in LBE is

$$\log c_{O,min} = 2.04 - \frac{8134}{T}. \tag{17}$$

The upper and lower limits of the oxygen concentration operational range, determined by the oxygen solubility in LBE and the magnetite formation oxygen potential, are given in Table 7. As shown in the table, the lower limit can be as low as $\sim 2.0 \times 10^{-4}$ ppm even at a high temperature of 600 °C, and the upper limit can be as high as ~ 1.03 ppm at a temperature 540 °C. This is at odds with experimental data. As summarized by Zhang and Li [58], if the oxygen concentration in LBE is as low as 1.0×10^{-4} in a flowing loop, it would be impossible to form a protective layer because of the two competing processes at the steel

Table 7 Operational range of oxygen concentration

Temperature (K)	Upper limited by solubility (ppm)	Lower limited by formation of magnetite (ppm × 10^6)
693	0.2973	3.24
713	0.4347	5.87
733	0.5646	1.03
753	0.6877	1.75
773	0.8044	29.0
793	0.9152	46.7
813	1.0205	73.7
833	1.1208	113.5
853	1.2164	171.6
873	1.3076	254.5

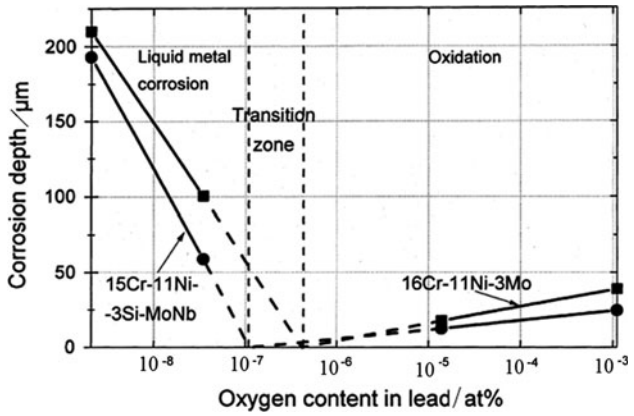

Fig. 7 Oxygen concentration effects on corrosion behavior of steels in flowing pure lead after 3,000 h at 823 K [59]

surface: dissolution and oxidation. The oxidation rate would be too low to form the protective layer. Based on Russian test results [59] as shown in Fig. 7, oxidation becomes excessive even the oxygen even is very below the solubility limit. At 550 °C (where the solubility is 1.2 ppm), when the oxygen concentration is set to be ~0.7 ppm, the corrosion rate by oxidation itself is ~0.2 mm year^{-1} which is too high to be acceptable. Therefore, using the solubility limit and the magnetite formation limit to determine the operational oxygen concentration range is not adequate.

The oxygen concentration range in LBE determined by the oxygen solubility and the magnetite layer formation was optimized by using the cladding temperature instead of using the coolant temperature [60, 61] which leads to an oxygen concentration range called as stability range as shown in Fig. 8. However, the stable range is still based on the solubility and the magnetite layer formation. The operation oxygen concentration should also depend on the flow

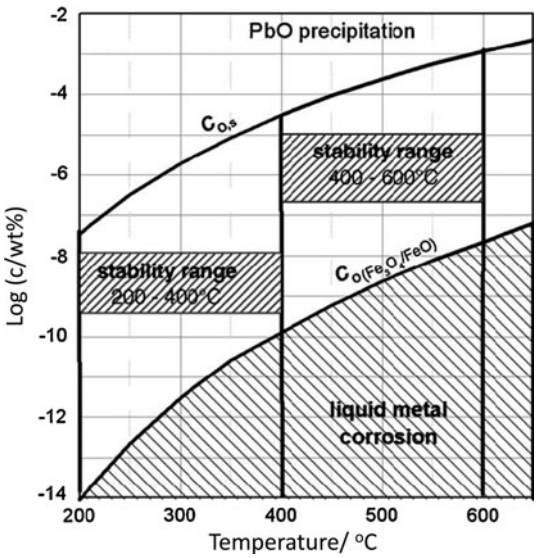

Fig. 8 Range between the solubility limit $c_{O,s}$ and the oxygen concentration at which decomposition of iron oxides takes place. The *areas between the curves* indicate the concentrations for which stable conditions are expected in a loop with the Pb Bi melt [60]

velocity [62] which affects the materials corrosion rates. The oxygen range with considering the effects of liquid metal flow and the materials composition was developed [63] as shown in Fig. 9. As shown in figure, for a reactor with an inlet temperature 460 °C and outlet temperature 550 °C, the oxygen concentration should be controlled to within a range of about 0.006–0.040 ppm for steel ss316. The range is much narrower than the range determined by the solubility and the concentration for magnetite formation. The range becomes narrower with increasing the outlet temperature of a reactor core for a given inlet temperature.

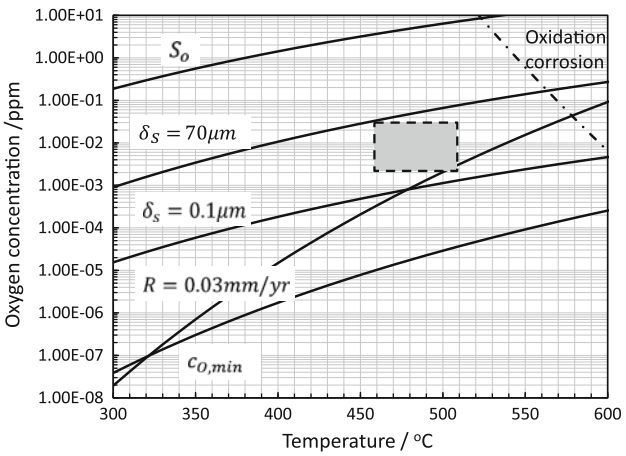

Fig. 9 Oxygen concentration range (*dark area*) needed to maintain a stable oxide film. The range is for a reactor core with 460 °C inlet and 520 °C outlet temperature. The data are based on an experimental corrosion correlation for SS 316. The flow velocity is 2 m s^{-1} and the hydraulic diameter is 0.05 m [63]. *R*, corrosion rate

6 Operation control method

There are three main methods to control the oxygen in LBE [10, 64]: direct injection of oxygen and hydrogen gases, injection of or using a cover gas of hydrogen and steam gas mixtures, and using PbO particles as solid phase control.

6.1 Direct injection of oxygen and hydrogen gases

Direct injection of oxygen and hydrogen gases mixed with an inert carrier gas (helium or argon) is a straight forward method to control the oxygen level in the liquid metal/alloy. The method has been applied in many liquid lead/LBE systems including test loops. The setup and procedures for this method are simple, and the input and output are in gaseous forms with no solid residues. Hydrogen can be directly injected into the flowing LBE or over a flowing LBE pool where the mass exchange rates are favorable, while oxygen should be only injected into cover gas spaces with great caution. The equilibrium states of the following reactions can be reached over time

$$\frac{1}{2}O_2 + H_2 \rightleftharpoons H_2O$$

$$\frac{1}{2}O_2(\text{gas}) \rightleftharpoons O(\text{dissolved in the liquid}).$$

Excess oxygen reacts with hydrogen to form steam. One of the main disadvantages of this method is that the very low oxygen partial pressure is very hard to be controlled. Slag can be formed at the injection area [65]. The mass exchange rate is also low between gas phase and liquid phase.

6.2 Injection of or using a cover gas of hydrogen and steam gas mixtures

The low oxygen concentration needed makes it nearly impossible to supply oxygen at the right level by injecting oxygen itself directly. However, such low concentration level can be achieved in a certain reaction system, e.g., hydrogen and water [8], or CO and CO_2 [66]. The former is particularly attractive since the hydrogen can also reduce PbO precipitation which is the main slag composition. For H_2/H_2O mixtures, the following reaction determines the oxygen partial pressure

$$\frac{1}{2}H_2 + O_2 \rightleftharpoons H_2O. \tag{18}$$

At the equilibrium

$$p_{O_2}^{\frac{1}{2}} = \frac{p_{H_2O}}{p_{H_2}} \exp\left(\frac{\Delta G_{H_2O}}{RT}\right). \tag{19}$$

Therefore, the ratio of H_2O to H_2 is related to the oxygen concentration in the liquid by

$$\log\left(\frac{p_{H_2O}}{p_{H_2}}\right) = 1.54 + \frac{4730}{T} + \log c_O \tag{20}$$

for LBE and

$$\log\left(\frac{p_{H_2O}}{p_{H_2}}\right) = -0.839 + \frac{6488}{T} + \log c_O \tag{21}$$

for liquid lead. Then we can get the required mixture of water and hydrogen for the formation of Fe_3O_4

$$\log\left(\frac{p_{H_2O}}{p_{H_2}}\right) = 1.25 - \frac{1645}{T} \tag{22}$$

and the required mixture for the precipitation of PbO (oxygen saturation) can be expressed

$$\log c_{O,\min} = 2.04 - 8134/T \tag{23}$$

for LBE and

$$\log\left(\frac{p_{H_2O}}{p_{H_2}}\right) = 2.36 + \frac{1388}{T} \tag{24}$$

for liquid lead.

In practical applications, a hydrogen and cover gas (He or Ar) mixture passes through a temperature-controlled water path to pick up steam at the desired levels [10]. The resultant hydrogen/steam mixture can either go directly into the LBE system to complete the reaction there, or go through a high temperature reaction chamber to reach thermodynamic equilibrium beforehand. Recently, study indicates that the method was quite an efficient way to control the oxygen in small loops, but was quite ineffective on larger facilities [67]. Other disadvantages of the method include slag formation by PbO precipitation and low mass exchange between gas and liquid phase [10].

6.3 Solid phase oxygen control

The main component of a solid phase oxygen control system is the mass exchanger [68]. The mass exchanger consists of a porous chamber filled with structurally stable PbO spherical particles. The system is installed in a by-pass loop at the coldest section of the non-isothermal LBE loop. When LBE flows through the porous structure PbO, it initially takes the oxygen out of the mass exchanger at a level equaling to the oxygen solubility at the temperature of the mass exchanger. The chemical reaction is

$$\text{PbO[solid]} \rightarrow \text{O[dissolved]} + \text{Pb[liquid]}. \tag{25}$$

It will reach its equilibrium with time, when the system has a uniform oxygen concentration. Therefore, by regulating the temperature and the LBE flow rate at the mass exchanger, the oxygen concentration in the non-isothermal LBE loop can be controlled to a desired level. However, considering the consumption of oxygen in the

system, the reaction (Eq. 25) will be always to the right side to supply oxygen for the main system.

This solid oxygen control method has been successfully applied to liquid lead–bismuth test loops [68, 69]. One example of the solid phase oxygen control system [68] is shown in Fig. 10. In this design, three hundred and sixty spherical PbO particles were mounted in each container between mesh plates in the reaction vessel, as shown in the figure. The sheathed heater was wound around the by-pass line, and the surface temperatures at several locations of the by-pass line were measured with sheathed thermocouples. In the reaction vessel, the sheathed heaters and the thermocouples were inserted for the temperature control and measurement in the liquid metal which contacts with the PbO particles. The outer surface of the reaction vessel was air-cooled to decrease the temperature of the melt in the vessel. The temperature of PbO was nearly equal to that of the melt because of high thermal conductivity of the liquid metal. The thermodynamic reaction (Eq. 25) of the dissolution of oxygen and the precipitation of the oxide occurs on the surfaces of the PbO particles and on the inner wall surface of the vessel.

For a given expected oxygen concentration, $c_{O,exp}$, the temperature at mass exchanger can be calculated

$$T_{MX} = \frac{3,400}{1.2 - \log c_{O,exp}}. \tag{26}$$

For the oxygen control range (0.006–0.04 ppm) in Fig. 9 for a non-isothermal LBE loop with a maximum temperature of 520 °C and minimum temperature of 460 °C, the temperature at the mass exchanger has to be controlled to within the range of 185–242 °C. Since the temperature at the mass exchanger is much lower than the temperature of the lowest temperature in the main flow path, corrosion fouling may happen in the mass exchanger, which can reduce the efficiency.

The time needed to achieve the desired oxygen concentration can be calculated if the total mass of LBE (m_{total}) and the mass flux through the mass exchange (f_{mMX}) are given

$$m_{total} c_{O,exp} = f_{mMx} t c_{O,exp}. \tag{27}$$

Then the time needed is expressed

$$t = \frac{m_{total}}{f_{mMx}}. \tag{28}$$

The dissociation of PbO releases liquid Pb into LBE, the total mass ($m_{Pb,rel}$) released is

$$m_{Pb,rel} = \frac{M_{Pb}(m_{total} c_{O,exp})}{100 M_O}, \tag{29}$$

where M_{Pb} and M_O are the atom weights of lead and oxygen, respectively. After the system reaches its equilibrium, the fraction of lead in the liquid metal is changed and can be estimated through

$$c_{Pb} = \frac{44.2 m_{total} + 100 m_{Pb,rel}}{m_{total} + m_{Pb,rel}}. \tag{30}$$

One operating condition (mass exchanger velocity = 0.1 m s^{-1}, flow path hydraulic diameter = 0.05 m, and total LBE in the loop 2 ton) has been calculated and the results are given in Table 8. The Pb fraction in LBE is increased by release of Pb into the system from the solid phase control. The fractional increase depends on the desired oxygen concentration. If the oxygen concentration is controlled to 0.038 ppm, the total release of Pb will be 9.9 kg with a consumption of 10.7 kg PbO. For this case, the fraction of Pb in LBE increases to 44.47 % from the original fraction of 44.2 %. The 0.27 % increase is small and should be acceptable.

The time needed for reaching the expected oxygen level throughout the loop depends on the total mass of LBE and the mass flux in the mass exchanger. As shown in Eq. 28, the time increases with the total mass and decreases with mass flux in the MX. For the calculated case, the time is

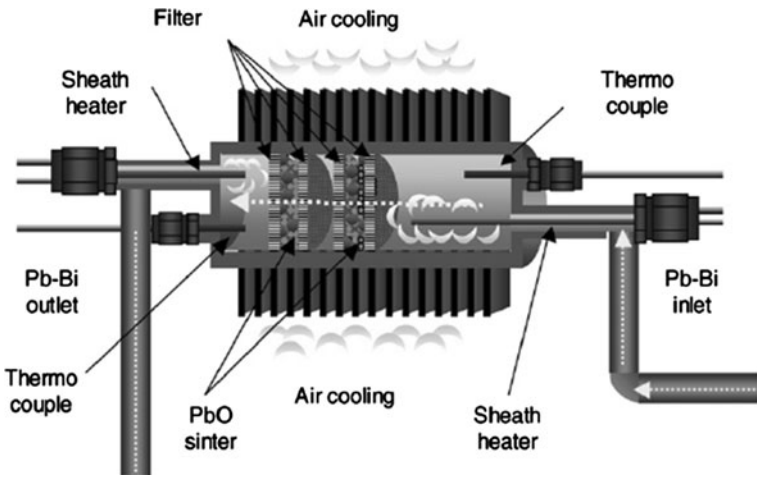

Fig. 10 Schematic of a solid oxygen control system [68]

Table 8 Calculated parameters for solid phase oxygen control for a condition with a flow velocity = 0.1 m s^{-1}, flow hydraulic diameter = 0.05 m, and total LBE in the system = 2 ton

Oxygen concentration (ppm)	Temp. at MX (K)	Flux at MX (kg s^{-1})	Time needed (h)	Total Pb release (kg)	Pb fraction (wt%)	PbO consumption (kg)
0.006	458	2.058	0.269735	1.564	44.24	1.68
0.01	472	2.056	0.270216	2.606	44.27	2.81
0.014	482	2.053	0.270550	3.649	44.30	3.93
0.018	489	2.051	0.270810	4.691	44.33	5.05
0.022	495	2.049	0.271024	5.734	44.36	6.17
0.026	501	2.048	0.271206	6.776	44.39	7.30
0.03	506	2.047	0.271365	7.819	44.42	8.42
0.034	510	2.046	0.271508	8.861	44.45	9.54
0.038	514	2.045	0.271636	9.904	44.47	10.66
0.042	517	2.044	0.271753	10.94	44.51	11.78

less than 20 min. If the flow velocity in the MX is reduced to 0.01 or 0.001 m s^{-1}, then the time will increase to $\sim$5 or 54 h, respectively. The temperature needed at the MX is determined only by the desired oxygen concentration. As shown in the table, the temperature at the MX is much lower than the lowest operating temperature in an LBE nuclear reactor coolant loop. For example, the minimum operating temperature is about 460 °C which is more 200° higher than the temperature at the MX even with the oxygen concentration is controlled to a value as high as 0.038 ppm.

It should be noted that the present calculations are assume that the oxygen concentration is uniform although the loop. However, in practice the oxygen concentration is non-uniform and is in a kinetic balance with structural materials and impurities in the LBE. Further investigation should be carried out on the oxygen kinetic and distribution effects on the oxygen control system.

The mass exchange between the solid and liquid is fast and this method can avoid slag formation [8], leading to cleaner operation over longer periods and less degradation of the thermal hydraulic performance. However, the solid phase oxygen control needs to install a fixed reserve of solid PbO, and if depleted, it is hard to replenish. The solid particles have to be kept mechanically and thermally stable [68].

7 Oxygen measurement

The method of the electromotive force (EMF) measurement with null current has been found to be an effective method to measure the oxygen concentration [70] in liquid lead and LBE, and the sensor technology has been well established [71–76]. The oxygen sensor can be expressed by the following cell:

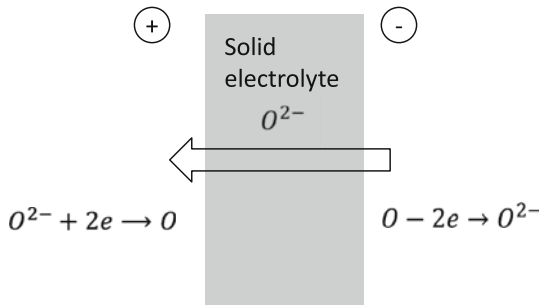

Fig. 11 A simple scheme of the working principle of an oxygen sensor

$$p_{O_2,1}//\text{solid electrolyte}//p_{O_2,2}, \tag{31}$$

where $p_{O_2,1}$ and $p_{O_2,2}$ are the oxygen partial pressure in each side of the solid electrolyte which is simply shown in Fig. 11. The materials for the solid electrolyte made of sintered ceramic of zirconic with addition of 8–19 % Yttria have a high conductivity of oxygen ions, while very low conductivity for electrons [72]. The oxygen ions flow from the high concentration side (or high chemical potential) to the low concentration side (or low chemical potential) through the solid electrolyte. Generally, metallic connection is used as electrodes for the both sides. The electrode at the high concentration side becomes positively charged due to the loss of the electrons, while the electrode at the low concentration side becomes negative charged due to the collecting the electrons as ions become oxygen atom or molecules. Therefore, an electro potential will be set up at equilibrium between the both sides.

After the equilibrium is set up, the EMF of the system can be calculated through the Nernst equation [27]

$$E = \frac{1}{2F}(\Delta\mu_{\text{ref}} - \Delta\mu_{\text{liquid}}), \tag{32}$$

where F is the Faraday constant, $\Delta\mu_{\text{ref}}$ and $\Delta\mu_{\text{liquid}}$ are the oxygen chemical potential of oxygen in the reference electrode and the in the liquid and

$$\Delta\mu_{\text{ref}} = \mu^0 + RT \ln a_{\text{o,ref}} \tag{33}$$

$$\Delta\mu_{\text{liquid}} = \mu^0 + RT \ln a_{\text{o,liquid}}. \tag{34}$$

The output signal can be obtained based on Eq. 32

$$E = \frac{RT}{4F} \ln\left(\frac{p_{\text{O}_2,\text{ref}}}{p_{\text{O}_2,\text{liquid}}}\right). \tag{35}$$

Therefore, the output signal depends on the reference system. The metal-oxide reference has been used in the development of oxygen sensors for heavy liquid metal technology. The oxygen partial pressure of a reference electrode relates with the standard Gibbs free energy of the formation of the corresponding oxide by Eq. 1. Considering Eqs. 13 and 14, the relationship between the output EMF (E) with a unity of mV and the oxygen concentration in the liquid can be expressed by

$$E = A_3 + B_3 + CT \log c_{\text{O}}, \tag{36}$$

where A_3, B_3, and C are constant. Equation 36 indicates that the output EMF has linear dependence on the temperature for a given oxygen concentration. The output EMF corresponds to the saturation limit and the concentration for formation of the protective layer (Fe_3O_4 formation) can be expressed by

$$E = A_4 + B_4 T. \tag{37}$$

The constants for various reference systems are given in Table 9. For example, the EMF range of a sensor with

Table 9 Calculated constants for EMF for various reference systems

	Bi_2O_3	PbO	In_2O_3	SnO_2	Air/pt
LBE					
A	−204.5	−331.6	−794.7	−702.8	803.22
B	0.072	0.0812	−0.077	0.394	−0.469
C	−0.099	−0.099	−0.099	−0.099	−0.099
Pb					
A	−379	−506.1	−969.1	−877.3	628.73
B	0.309	0.3174	0.1589	0.63	−0.233
C	−0.099	−0.099	−0.099	−0.099	−0.099
LBE saturate					
A	132.8	5.7854	−457.3	−365.5	1,140.6
B	−0.047	−0.038	−0.196	0.275	−0.588
Pb saturate					
A	127	−0.019	−463.1	−371.3	1,134.8
B	−0.009	−2E−04	−0.159	0.313	−0.55
For Fe_3O_4 formation					
A	398.3	271.26	−191.8	−99.98	1,406.1
B	0.102	0.1105	−0.048	0.423	−0.439

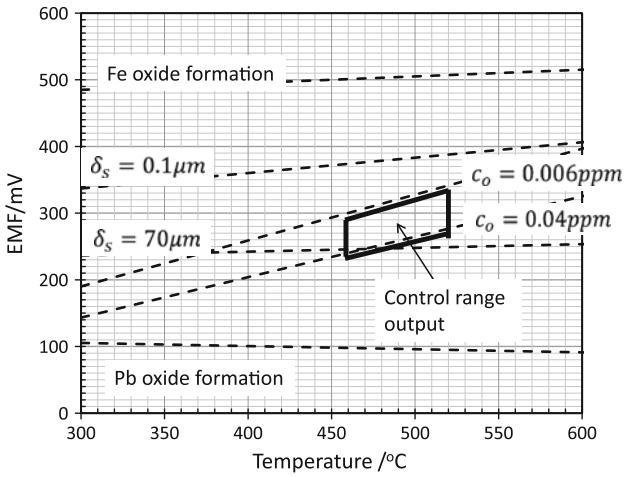

Fig. 12 Sensor output including EMF for the oxygen control range in Fig. 9

Bi_2O_3/Bi as reference corresponding to Fig. 9 is given in Fig. 12.

8 Issues and solution in oxygen control technology

Oxygen control technology was initially developed in Russia and has been successfully applied in their nuclear power submarines to protect the structural materials from LBE corrosion. In last decades, it has been studied worldwide for applications in accelerator driven systems and advanced nuclear reactors. However, issues remain for successful application of oxygen control technology in an LBE system. The issues and potential solutions are summarized in Table 10.

9 Other corrosion inhibitors for liquid lead and LBE

Liquid lead and LBE have been considered as a coolant in nuclear reactor applications for more than 50 years. The early studies on reducing the corrosion rate focused on development of metallic inhibitors. Zr and Ti have been found to be effective corrosion inhibitors of steels exposing to liquid lead and lead bismuth [77].

9.1 Inhibition mechanism

Metallic inhibitor (Ti and Zr) in liquid lead and LBE inhibits the corrosion through reactions at the steel surface with minor constituents (N and C) of the steel. The reaction produces a surface layer composed of (Ti, Zr)N or (Ti, Zr)C, which severs as a barrier to prevent dissolution of the steel components. Therefore, any factor that affects the N and C activities in the steel will affect the inhibition efficiency [3].

Table 10 Oxygen control: issues, status, and further studies

Issues	Status	Further studies needed
Operational oxygen concentration range	In most studies, the upper limit of oxygen concentration is set by the oxygen solubility limit and the lower limit is set by the formation of a Fe_3O_4 oxide layer. However, experiments have shown that even if the oxygen concentration is controlled to a value where theory says the oxide layer can be formed, extensive dissolution corrosion can occur because the layer is not stable. Further, at a high enough oxygen level (but below the solubility limit), sufficient oxidation can occur to damage the structural materials	The reasonable operational oxygen range should be identified based on the oxide layer stable range. The oxide layer should not be thick enough for spallation to occur or too thin to be protective. The spallation limit of oxide in LBE and the continuous oxide layer formation limit have to be identified experimentally or theoretically
Protective layer stability	Present studies indicate that a stable protective layer can be formed on a steel surface if the temperature is below 550 °C and if the oxygen concentration is controlled to about 0.01–0.05 ppm. There are no data on the protective layer stability under either irradiation or other LBE environments, and there has been no study in the US for mechanical erosion of the protective coating	Experimental studies should be carried on the stability of the protective oxide layer under irradiation in LBE, and theoretical investigation is needed to identify the LBE mechanical damage to the protective layer
Oxygen measurement	An oxygen sensor has been developed. Materials for the sensor are Yittria stabilized ZrO_2 for the electrolyte, Mo for the wire, and Bi/Bi_2O_3 for the reference. The sensor has been calibrated, and has been operated for several thousands of hours. The experimental outputs agree very well with the theoretical correlations	At least one experiment should be run to identify the long-term behavior of the developed oxygen sensor
Oxygen control method	Three methods have been developed: injection of H_2/O_2 gas mixtures with inert gas, injection of H_2/steam gas mixtures with inert gas and solid phase control using PbO particles. All of them have disadvantages and advantages. Solid phase control is preferred for the hyperion reactor	A mass exchanger with stability (mechanical and thermal) and efficiency should be developed. The non-uniform oxygen distribution, the interactions of oxygen with other impurities, and corrosion fouling effects on control system have to be identified, as well as PbO dissolution kinetics
Interactions between the oxygen and other impurities	There are available studies on interactions between oxygen and hydrogen in LBE	Coolant chemistry is one of the main tasks for development of LBE coolant technology

The stability of possible nitrides [78] in steels can be ranked as: $ZrN > TiN > AlN > TaN > VN > Si_3N_4 > Mn_xN_y > Cr_2N > Mo_2N$. Therefore, adding Ti and Zr into the liquid lead and lead–bismuth alloy can result in the most stable nitrides if nitrogen can be supplied from the solid steel. Considering that Zr, Ta, and Ti are not commonly presented in steels, then increasing any of the left elements (Al, V, Si, Mn, Mo, Cr) will reduce the activity of N in the steel and affect the formation of the protective layer [78]. when $N/Al < 1$ in the steel and the heat treatment history has favored precipitation of AlN, the surface films formed on both carbon and low alloy steels have been found to be (Zr, Ti)C [78]. Also, the nitride layer can be converted to a carbide layer by depletion of N through reaction with the inhibitor.

For protective carbide layer, there is a critical C concentration below which the inhibition efficiency is low [78]. The critical concentration is close to the value required to form $Cr_{23}C_6$, which indicates that the excess carbon above the critical concentration is beneficial to the inhibition film formation. Based on the comparisons between experimental results in a liquid bismuth environment and theoretical predictions, Weeks and Klamut [78] concluded that the formation of nitride film was controlled by the nitrogen diffusion in the film, while the formation of carbide film was controlled by the carbon diffusion in the steel.

The required concentration of zirconium in the liquid is slightly easier to be maintained than that of titanium, and also zirconium has a lower thermal neutron cross-section than titanium. Therefore, Zr appears to be the better effective inhibitor compared with Ti [77].

9.2 Inhibition efficiency

Table 11 gives test results of Croloy 1-1/4 steel in flowing LBE (summarized by Park et al. [77], original data by Romano et al. [79]). Without inhibitor addition, severe

Table 11 Corrosion of Croloy 1-1/4 steel in flowing LBE

Temperature (K)	Test time (h)	Inhibitor condition	Corrosion results
773–898	<1,000	No inhibitor	Severe corrosion
673–823	1,000–5,000	No inhibitor	Severe corrosion
898	<100	No inhibitor	Severe corrosion
623–923	<5,000	Ti added	No corrosion
773–923	<10,000	Zr added	No Corrosion

corrosion was found even that the experiment only lasted 100 h, while with Ti and Zr addition, no corrosion was observed after testing 10,000 h. Figure 13 shows an example of surface change of steel exposed to LBE with and without inhibitor addition [80]. The figure shows that no corrosion attack layer can be observed after 6,000 h exposure in LBE with 10–40 ppm Ti addition, while the corrosion attack layer is more than 40 μm after only 300 h exposure without inhibitor addition.

Considering that the protective layer is formed by the chemical reactions between the inhibitor (Ti or Zr) in the liquid with carbon or nitrogen or both in the steel, the content of N and C in the steel can affect the inhibition efficiency. Corrosion results [81] of iron with different C and N contents in liquid bismuth at a temperature of 750 °C are given in Table 12. Except the sample with 0.21 % N, the weight loss of other samples decreases with the total content of C and N increasing. However, as indicated in the Ref. [81], the carbon seems to be more efficient than nitrogen as shown in the table.

The inhibition efficiency also depends on the alloying constituents of the steel, such as Al, Cr, Si, and Mn, because all metallic constituents can reduce N and C activities. For carbon steels, the efficiency can be above 95 %, while for stainless steel (19Cr–8Ni), the efficiency is reduced to 55 % in liquid lead. As summarized in a review publication [3], Zr and Ti are effective metallic inhibitors for carbon and low alloy steels exposure to liquid lead and lead–bismuth, while for stainless steels the inhibition efficiency is low.

Table 12 Weight loss of iron after 2-week exposure to inhibited bismuth at temperature 1,023 K

Carbon (%)	Nitrogen (%)	Total C + N (%)	Corrosion, weight loss (mg)
0.0041	0.0288	0.6980	170
0.085	0.0288	0.1138	30
0.234	0.0288	0.2628	<1
0.0041	0.385	0.0426	141
0.0041	0.3100	0.3141	33

9.3 Inhibitor control and critical concentration

The inhibitor concentration must be properly controlled, or the inhibition efficiency could be reduced. Continuing adding inhibitors during operation is necessary to maintain the protective layer or reform new layers at locations where protective layer failures such as spallation occur [77]. Any failure of the protective layer can result in severe pitting corrosion [78].

For avoiding oxidation of inhibitors, oxygen getter such as Mg and Ca must also be added to the liquid metal/alloy, or the inhibitor can be oxidized and a layer composed of oxide–nitride compounds will be formed at the surface which has been found not to be tightly adhered and it is liable to break away [6]. The concentration of the oxygen getter should be kept below 1,000 ppm to avoid suppression of zirconium solubility in the liquid metal and possible inter-metallic compound formation [77].

Solubility of Ti and Zr in liquid lead–bismuth has been measured as a function of temperature [82]. The solubility can be expressed by

$$\log S = A_5 + \frac{B_5}{T}, \tag{38}$$

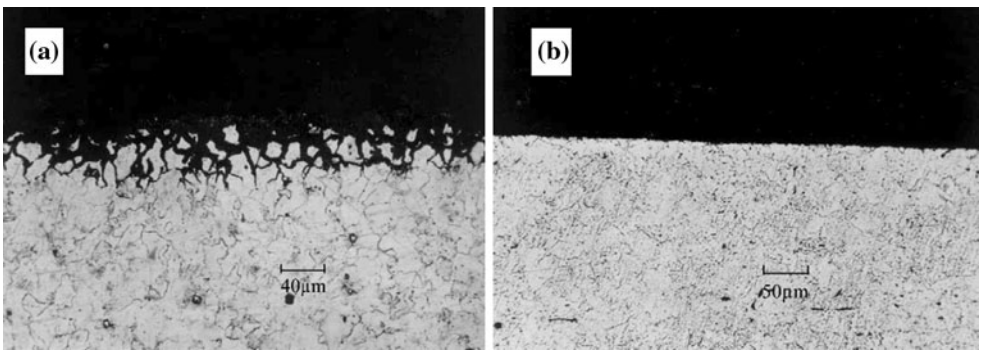

Fig. 13 Microphotography of **a** attack of 2 CrSiMoV steel after 300 h in LBE without inhibitor and **b** protect of CrMoV steel after 6,000 h in LBE with 10–40 ppm Ti. The experiments were carried out at 873 K with 300–500 Mg added for oxygen getter [80]

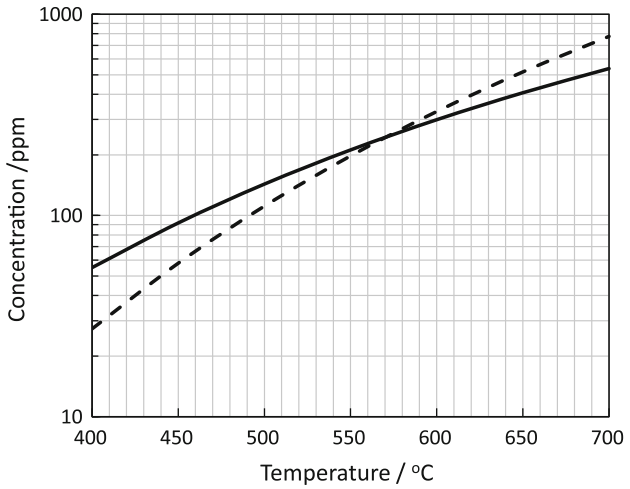

Fig. 14 Solubility curves of Ti and Zr in liquid lead–bismuth

where T is the temperature in Kelvin. For Ti, $A_5 = 4.95$ and $B_5 = -2{,}160$ in the temperature range of 285–700 °C. For Zr, $A_5 = 6.15$ and $B_5 = -3{,}172$ in the temperature range of 350–750 °C. The solubility curves are given in Fig. 14.

The inhibitor concentration range in which the inhibition has the best efficiency has not been determined yet. Most of the available experimental tests were carried out with concentration of the inhibitor less than 500 ppm [83]. Considering that the kinetics of the chemical reactions for film formation and film properties are temperature dependent, the ideal range of the concentration of the inhibitor should also depend on the operation temperature. Ilincev [80] concluded that the inhibitor can prevent corrosion almost completely at temperatures below 700 °C and partly in the temperature range of 700–800 °C.

10 Conclusion

Corrosion of stainless steels by liquid lead and LBE can be significantly mitigated by applying oxygen control technology. The corrosion inhibition efficiency of the technology depends on not only the oxygen concentration in the liquid but also the type of structural steels as well the system operating conditions. For maintaining the protective films formed through reactions between oxygen and steel constituents and also avoiding contamination of the liquid, the oxygen concentration must be controlled in a certain range. The oxygen control technology, including oxygen measurement and control methods, has been well developed. However, more studies are needed to determine the reasonable operating range of oxygen concentration in a non-isothermal loop system. The present study also addresses metallic inhibitors (Zr and Ti) which are effective metallic inhibitors for carbon and low alloy steels exposure to liquid lead and lead–bismuth, while for stainless steels the inhibition efficiency is low.

References

1. Gromov BF, Orlov YI, toshinskii GI, Chekunov VV (1996) Nuclear power plants with lead–bismuth coolant. At Energy 81(5):770–775
2. Kurata Y, Futakawa M, Kikuchi K, Satito S, Osugi T (2002) Corrosion studies in liquid Pb–Bi alloy at JAERI: R&D program and first experimental results. J Nucl Mater 301:28–34
3. Zhang J (2009) A review of corrosion by liquid lead and lead–bismuth. Corros Sci 51(6):1207–1227
4. Zhang J, Li N (2003) Parametric study of a corrosion model applied to lead–bismuth flow system. J Nucl Mater 321:184–191
5. Lyutyi EM (1987) Problems of high temperature liquid metal corrosion of refractory metals and alloys. Mater Sci 24(5): 441–445
6. Loewen EP, Yount HJ, Volk K, Kumar A (2003) Layer formation on metal surfaces in lead–bismuth at high temperatures in presence of zirconium. J Nucl Mater 321:269–280
7. Kurata Y, Sato H, Yokota H, Suzuki T (2011) Applicability of Al-powder-alloy coating to corrosion barriers of 316SS in liquid lead bismuth eutectic. Mater Trans 52:1033–1044
8. Li N (2002) Active control of oxygen in molten lead–bismuth eutectic systems to prevent steel corrosion and coolant contaminations. J Nucl Mater 300:73–81
9. Loewen EP, Tokuhiro AT (2003) Status of research and development of lead-alloy-cooled fast reactor. J Sci Technol 40:614–627
10. Li N (2008) Lead-alloy coolant technology and materials–technology readiness level evaluation. Prog Nucl Energy 50:140–151
11. OECD Nuclear Energy Agency (2007) Handbook on lead–bismuth eutectic alloy and lead properties, materials compatibility, thermal-hydraulics and technologies. OECD Nuclear Energy Agency, Paris
12. Gromov BF, Orlov YI, Martynov PN, Gulevsky VA (1998) The problems of technology of the heavy liquid metal coolants (lead–bismuth, lead). In: Proceedings of heavy liquid metal coolants in nuclear technology (HLMC-98), vol 1, p 87
13. Gannesan R, Gnansekaran T, Srinivasa RS (2002) Standard molar Gibbs free energy of formation of PbO (s) over a wide temperature range from EMF measurements. J Nucl Mater 320:258–264
14. Gannesan R, Gnansekaran T, Srinivasa RS (2003) Determination of standard molar Gibbs free energy of formation of Bi_2O_3 over a wide temperature range by EMF method. J Chem Thermodyn 35:1703–1716
15. Samsonov GV (ed) (1982) The oxide handbook, 2nd edn. IFI/Plenum, New York
16. Chang AY, Fitzner K, Zhang M (1988) The solubility of gases in liquid metals and alloys. Prog Mater Sci 32(2):97–259
17. Ganesan R, Gaanasekaran T, Srinivas RS (2006) Diffusivity, activity and solubility of oxygen in liquid lead and lead–bismuth eutectic alloy by electrochemical methods. J Nucl Mater 349: 122–149
18. Heshmatrour B, Stevenson DA (1981) An electrochemical study of the solubility and diffusivity of oxygen in the respective liquid metals indium, gallium, and bismuth. J Electroanal Chem 130: 47–55
19. Alcock CB, Belford TN (1964) Thermodynamics + solubility of oxygen in liquid metals from EMF measurements involving solid electrolytes. 1. Lead. Trans Faraday Soc 60:4975

20. Fitzner K (1980) Diffusivity, activity and solubility of oxygen in liquid bismuth. Thermochim Acta 35:277–286
21. Szwarc R, OberG KE, Rapp RA (1972) The diffusivity and solubility of oxygen in liquid lead from electrochemical measurements. High Temp Sci 4:347–356
22. Martynov PN, Ivanov KD (1997) Properties of lead–bismuth coolant and perspectives of non-electric applications of lead-bismuth reactor. In: IAEA-TECDOC-1056, pp 177–184
23. Kishimoto A, Wada A, Michimoto T, Furukawa T, Aoto k, Oishi T (2006) Solubility and activity of oxygen in Pb–Bi melts. Mater Trans 47:122–128
24. Anik S, Frohberg MG (1987) Thermodynamics and solubility of oxygen in liquid bismuth–lead and bismuth–antimony alloys. Ber Bunsenges Phys Chem 91:790–794
25. Taskinen A (1982) Activity coefficient of oxygen in Pb–Bi and Pb–Sb melts. Z Für Metall 73:163–168
26. Otsuka S, Kurose Y, Kozuka A (1984) Activities of oxygen in liquid Bi–Pb and Bi–Sb alloys. Metall Trans B 158:141–146
27. Zhang J, Li N, Chen Y (2006) Oxygen control technique in molten lead and lead–bismuth eutectic system. Nucl Sci Eng 154:223–232
28. Steiner H, Schroer C, Vob Z, Wedemeyer O, Konys J (2008) Modeling of oxidation of structural materials in LBE systems. J Nucl Mater 374:211–219
29. Zhang J, Kapernick R (2009) Oxygen chemistry in liquid sodium–potassium systems. Prog Nucl Energy 51:614–623
30. Martynov PN, Orlov YI (1998) Slagging processes in lead–bismuth: prevention and elimination of critical situations. In: Proceedings of heavy liquid metal coolants in nuclear technology (HLMC-98), vol 2, p 665
31. Zhang J, Li N, Chen Y (2005) Dynamics of high temperature oxidation accompanied by scale removal and implications for technological applications. J Nucl Mater 342:1–7
32. Schroer C, Skrypnik A, Wedemeyer O, Konys J (2012) Oxidation and dissolution of iron in flowing lead–bismuth eutectic at 450°C. Corros Sci 61:63–71
33. Furukawa T, Muller G, Schumacher G, Weisenburger A, Heinzel A, Zimmermann F, Aoto K (2004) Corrosion behavior of FBR candidate materials in stagnant Pb–Bi at elevated temperature. J Nucl Sci Technol 41:265
34. Briceno DG, Crespo LS, Munoz FJM, Hernandez Arroyo F (2002) Influence of temperature on the oxidation/corrosion process of F82Hmod. martensitic steel in lead–bismuth. J Nucl Mater 303:137
35. Zhang J, Li N (2005) Oxidation mechanism of steels in liquid-lead alloys. Oxid Met 63:353–381
36. Robertson J (1991) The mechanism of high temperature aqueous corrosion of stainless steels. Corros Sci 32:443–465
37. Martinelli L, Jean-Louis C, Fanny B-C (2011) Fanny, Oxidation of steels in liquid lead bismuth: oxygen control to achieve efficient corrosion protection. Nucl Eng Des 241:1288–1294
38. Martinelli L, Fanny BC, Picard G, Santarini G (2008) Oxidation mechanism of an Fe–9Cr–1Mo steel by liquid Pb–Bi eutectic alloy at 470° C (Part III). Corros Sci 50:2523–2536
39. Rowlands DGPC, Humphrey P (1988) Growth mechanisms of oxides formed on Fe–9Cr steel in high pressure carbon dioxide studied using imaging SIMS. Mater Sci Technol 4:1117
40. Forrest JE, Robertson J (1991) Corrosion of Cr steels in high temperature acid chloride solutions. Corros Sci 32:541–561
41. Zhang J, Li N, Chen Y, Rusanov AE (2005) Corrosion behaviors of US steels in flowing lead–bismuth eutectic. J Nucl Mater 336:1–10
42. Tsisar V, Yeliseyeva O (2007) Oxidation of Armco-Fe and steels in oxygen saturated liquid lead. Mater High Temp 24(2):93–101
43. Short MP, Ballinger RG, Hanninen HE (2013) Corrosion resistance of alloys F91 and Fe–12Cr–2Si in lead–bismuth eutectic up to 750°C. J Nucl Mater 434:259–281
44. Zhang J, Hosemann P, Maloy S (2010) Models of liquid metal corrosion. J Nucl Mater 404:82–96
45. He X, Li N, Mineev M (2001) A kinetic model for corrosion and precipitation in non-isothermal LBE flow loop. J Nucl Mater 297:214–219
46. Fazio C, Benamati G, Martini C, Palombarini G (2001) Compatibility tests on steels in molten lead and lead–bismuth. J Nucl Mater 296:243–248
47. Muller G, Schumacher G, Zimmermann F (2000) Investigation on oxygen controlled liquid lead corrosion of surface treated steels. J Nucl Mater 278:85–95
48. Glasbrenner H, Konys J, Mueller G, Rusanov A (2001) Corrosion investigations of steels in flowing lead at 400°C and 550°C. J Nucl Mater 296:237–242
49. Gorynin IV, Karzov GP, Markov VG, Lavrukhin VS, Yakovlev VA (1998) Structure materials for power plants with heavy liquid metals as coolants. In: Proceedings of heavy liquid metal coolants in nuclear technology (HLMC-98), vol 1, p 120, Obninsk, Russia
50. Barbier F, Benamati G, Fazio C, Rusanov A (2001) Compatibility tests of steels in flowing liquid lead–bismuth. J Nucl Mater 295:149–156
51. Illincev G, Karnik D, Paulovic M, Doubkova A (2004) The impact of the composition of structural steels on their corrosion stability in liquid Pb–Bi at 500 and 400°C with different oxygen concentrations. J Nucl Mater 335:210–216
52. Barbier F, Rusanov A (2001) Corrosion behavior of steels in flowing lead–bismuth. J Nucl Mater 296:231–236
53. Muller G, Heinzel A, Konys J, Schumacher G, Weisenburger A, Zimmermann F, Engelko V, Rusanov A, Markov V (2002) Results of steel corrosion tests in flowing liquid Pb/Bi at 420–600°C after 2000 hours. J Nucl Mater 301:40–46
54. Deloffre P, Balbaud-Celerier f, Terlain A (2004) Corrosion behavior of aluminized martensitic and austenitic steels in liquid Pb–Bi. J Nucl Mater 335:180–184
55. Kondo M, Takahashi M (2006) Corrosion resistance of Si- and Al-rich steels in flowing lead–bismuth. J Nucl Mater 356: 203–212
56. Allen TR, Crawford DC (2007) Lead-cooled fast reactor systems and the fuels and materials challenges. Sci Technol Nucl Install ID 97486. doi:10.1155/2007/97486
57. Lai GY (2007) High-temperature corrosion and materials applications. ASM International, Materials Park
58. Zhang J, Li N (2008) Review of the studies on fundamental issues in LBE corrosion. J Nucl Mater 373:351–377
59. Gorynin IV, Karzov GP, Markov VG, Lavrukhin VS, Yakovlev VA (1998) In: Proceedings of heavy liquid metal coolants in nuclear technology (HLMC-98), vol 1, p 120, Obninsk, Russia
60. Muller G, Heinzel A, Schumacher G, Weisenburger A (2003) Control of oxygen concentration in liquid lead and lead–bismuth. J Nucl Mater 321:256–262
61. Courouan JL, Robin JC (2004) Chemistry control analysis of lead alloys systems to be used as nuclear coolant or spallation target. J Nucl Mater 335:264–269
62. Ballinger RG, Lin J (2004) An overview of corrosion issues for the design and operation of high-temperature lead- and lead–bismuth-cooled reactor systems. Nucl Technol 147:418–435
63. Zhang J (2010) Preliminary analysis of lead bismuth eutectic technology for application of HYPERION reactor. Report to LANL, LA-UR-10-01476
64. Li N, Darling T (2002) Oxygen control methodology and calibration strategy. Report, Los Alamos National Laboratory, LA-UR-02-4447
65. Hata K, Takahashi M (2003) Experimental study on oxygen potentials in liquid lead–bismuth eutectic, Global 2003. In: ANS/ENS international winter meeting, Now Orleans, 16–20 Nov 2003

66. Muller G, Schumacher g, Zimmermann F (2000) Investigation on oxygen controlled liquid lead corrosion of surface treated steels. J Nucl Mater 278:89
67. Brissonneau L, Beauchamp F, Morier O, Schroer C, Konys J, Kobzova A, Di Gabriele F, Courouau J-L (2011) Oxygen control systems and impurity purification in LBE: learning from DEMETRA project. J Nucl Mater 415:344–360
68. Kondo M, Takahashi M, Miura K, Onizawa T (2006) Study on control of oxygen concentration in lead–bismuth flow using lead-oxide particles. J Nucl Mater 357:97–104
69. Rusanov AE, Demishonkov AP (2000) Results of corrosion tests of 316, 316L, T-410, HT-9 and d-9 steels. Technical Report to Los Alamos National Laboratory under Contract #H12030008-35 between SSCRF IPPE (Russian) and LANL (U.S.A)
70. Courouan JL, Deloffre P, Adriano R (2002) Oxygen control in lead–bismuth eutectic: first validation of electrochemical oxygen sensors in static conditions. J Phys IV France 12(Pr8): 141–153
71. Darling TW, Li N (2002) Oxygen concentration measurement in liquid Pb–Bi Eutectic. Report to Los Alamos National Laboratory, LA-UR-02-3036
72. Khalid Rivai A, Kumagai T, Takahashi M (2008) Performance of oxygen sensor in lead–bismuth at high temperature. Prog Nucl Energy 50:575–581
73. Fernandez JA, Abella J, Barcelo J, Victori L (2002) Development of an oxygen sensor for molten 44.5% lead–55.5% bismuth alloy. J Nucl Mater 301:47–52
74. Konys J, Muscher H, Voß Z, Wedemeyer O (2001) Development of oxygen meters for the use in lead–bismuth. J Nucl Mater 296:289–294
75. Courouan JL (2004) Electrochemical oxygen sensors for on-line monitoring in lead–bismuth alloys: status of development. J Nucl Mater 335:254–259
76. Kondo M, Takahashi M, Miura K, Onizawa T (2006) Study on control of oxygen concentration in lead–bismuth flow using lead oxide particles. J Nucl Technol 357:97–104
77. Park JJ, Butt DP, Beard CA (2000) Review of liquid metal corrosion issues for potential containment materials for liquid lead and lead–bismuth eutectic spallation targets as a neutron source. Nucl Eng Des 196:315–325
78. Weeks JR, Klamut CJ (1960) Reactions between steel surfaces and zirconium in liquid bismuth. Nucl Sci Eng 8:133–147
79. Romano AJ, Klumet CJ, Gurinsky DH (1963) The investigation of container materials for Bi and Pb alloys. Part I. Thermal convection loops. Brookhavern National Laboratory Report, BNL-811
80. Ilincev G (2002) Research results on the corrosion effects of liquid heavy metals Pb, Bi and Pb–Bi on structural materials with and without corrosion inhibitors. Nucl Eng Des 217:167–177
81. James JA, Trotman J (1960) Corrosion of steels in liquid bismuth and lead. J Iron Steel Inst 194:319–323
82. Weeks J, Romano AJ (1969) Liquid curves and corrosion of Fe, Ti, Zr, and Cu in liquid Bi–Pb alloys. Corrosion 25:131–136
83. Epstein LF (1957) Static and dynamic corrosion and mass transfer in liquid metal systems. Chem Eng Prog 53:67–81